

Short Communication

Enhanced Activity for Methanol Electro-oxidation on PtRu/C Catalyst by Reduction Treatment

Qi Wang^{*}, Hualong Tao, Zhiqiang Li, Liu Shanshan, Lei Han

College of Materials Science and Engineering, Dalian Jiaotong University, Dalian 116028, Liaoning, China

*E-mail: qiwang@djtu.edu.cn

Received: 29 March 2017 / Accepted: 9 May 2017 / Published: 12 June 2017

Modified ethylene glycol method was used to synthesize PtRu/C catalyst which then annealed at different temperatures in hydrogen atmosphere. By X-ray diffraction, scanning and transmission electron microscopy, energy dispersive spectroscopy and inductively coupled plasma atomic emission spectroscopy, the structure and composition of catalysts were analyzed; Simultaneous thermal analysis tests gave the mass loss and thermal effect of the catalysts. Electrochemical methods were used to evaluate electro-catalytic activity of the catalysts towards CO and methanol electro-oxidation. The results showed that the average particle size and PtRu alloy crystallinity increased during the reduction treatment. Most of the surface adsorption species were removed after reduction treatment at 300 °C due to the decomposition temperature ranges of 110 ~ 220 °C. The catalyst with reduction treatment at 300 °C exhibited the highest electrocatalytic activities, which was attributed to the removal of adsorption species, the increase of crystallinity and the formation of grain boundary.

Keywords: PtRu/C; reduction treatment; electro-catalytic activity; methanol electro-oxidation; CO tolerance

1. INTRODUCTION

An effective electro-catalyst is important as the key material of fuel cells, which attracts much attention in energy conversion field. In the development of fuel cell catalysts, the problem of carbon monoxide (CO) poisoning still can't be ignored [1-3]. Binary PtRu are often considered as superior and stable catalysts for CO-containing hydrogen and methanol electro-oxidation [4-7]. Bifunctional mechanism and ligand effect are proposed as the interpretation of improved CO tolerance on PtRu catalyst [8-13]. The bifunctional mechanism is attributed to the facilitation of CO_{ads} oxidation on Pt in the presence of Ru by producing oxygen containing species and the ligand effect declares that the

alloying of Pt with Ru makes electronic structure of Pt modified, which weakens CO adsorption on Pt. Therefore, the electrochemical activity of PtRu/C catalysts is related closely to its surface composition, the particle size, grain boundary, and the PtRu crystallinity, which were greatly affected by preparation methods.

Polyol process has been widely employed in preparing PtRu/C catalysts among the various approaches such as impregnation, sol-gel, electrodeposition and liquid colloidal methods due to the advantages of simply operation, small particle size and uniform distribution of nanoparticles [14-18]. Meanwhile, ethylene glycol can be oxidized to be glycolic acid or its anion (glycolate) during the reduction process of metal ions, which could adsorb on the catalyst surface, resulting in the decrease of catalytic activity [16, 19, 20]. In addition, element analysis indicates that the content of RuO_x is higher than metallic Ru in the catalyst prepared by polyol method [21, 22]. The excess oxides of Pt and Ru may decrease the utilization of PtRu alloy catalyst although suitable oxides are in favor of the electro-oxidation of CO and methanol [22]. Therefore, PtRu/C catalyst was prepared in this paper using ethylene glycol method followed by reduction treatment at different temperatures to modify the catalyst particle size and grain boundary, alloy degree, surface composition and oxidation state of Pt and Ru, finally to improve the electrochemical activities for CO and methanol electro-oxidation.

2. EXPERIMENTAL

2.1 Catalyst preparation

$\text{H}_2\text{PtCl}_6 \cdot 6\text{H}_2\text{O}$ and $\text{RuCl}_3 \cdot x\text{H}_2\text{O}$ with 37 wt. % of Ru content were used as the catalyst precursors and commercial Vulcan XC-72R was adopted as the support material. The catalyst metal loading was 45 wt% with an atomic Pt/Ru ratio of 2. The calculated amounts of $\text{H}_2\text{PtCl}_6 \cdot 6\text{H}_2\text{O}$ and $\text{RuCl}_3 \cdot x\text{H}_2\text{O}$ was dissolved in ethylene glycol respectively, and then they were mixed in a three-necked flask. 1 mol L^{-1} NaOH solution was also added to the flask to adjust the pH value. The solution was then heated to $165 \text{ }^\circ\text{C}$ from room temperature and kept at the temperature for 4 h, followed by cooling to $90 \text{ }^\circ\text{C}$. 1.5 mol L^{-1} HCl was added to the flask to adjust the pH to 2. After 24 h at $90 \text{ }^\circ\text{C}$, the obtained catalyst was filtered and washed by hot water. Finally, the catalyst was dried at $80 \text{ }^\circ\text{C}$ for 10 h in a vacuum oven. The obtained PtRu/C catalyst was treated for 2 hours in reducing atmosphere (5 vol. % H_2 in argon) at $150 \text{ }^\circ\text{C}$, $300 \text{ }^\circ\text{C}$ and $450 \text{ }^\circ\text{C}$, respectively. The final catalyst was donated as PtRu/C-150, PtRu/C-300 and PtRu/C-450, respectively.

2.2 Physicochemical characterization

X-ray diffraction (XRD) patterns of all the samples were obtained with an Empyrean X-ray diffractometer using Cu K α radiation. The 2θ angular scan was from 10° to 90° with a scan rate of 0.2° s^{-1} . The tube current was 40 mA and tube voltage was 40 kV. Catalyst morphology was observed using a JSM 2100F transmission electron microscopy (TEM). The sizes of 200 particles were measured. The particle size distribution and average particle size of the catalysts were calculated based

on the measurement. X-ray energy dispersive spectroscopy (EDS) analysis was also applied to analyse the element composition of the catalysts. Inductively coupled plasma optical emission spectroscopy (ICP-OES) analysis was carried out using Leeman Prodigy instrument with the pre-treatment of calcination and acid dissolution. Simultaneous thermal analysis (STA) with 449F3 model in Germany was used to analyse mass loss and heat effect of the catalysts.

2.3 Electrochemical measurements

Electrochemical measurements were carried out on Princeton PARSTAT.2273 working station at room temperature (20 °C). A glassy carbon (GC) electrode ($\Phi = 6$ mm) covered by the prepared catalyst was used as working electrode [23]. Pt sheet was used as a counter electrode and saturated calomel electrode (SCE) as a reference electrode. While all the potential values in this paper were referred to reversible hydrogen electrode (RHE). Pure CO was bubbled in 0.1 mol L⁻¹ HClO₄ for 10 min during CO stripping voltammetry experiment. High-purity Argon was used to remove the residual CO which dissolved in the solution. Linear sweep voltammetry (LSV) experiments towards methanol electro-oxidation was carried out from 0 to 0.66 V with 1 mV s⁻¹ scan rate in 0.1 mol L⁻¹ HClO₄ and 0.5 mol L⁻¹ CH₃OH. The chronoamperometry curves (CA) were recorded at 0.7 V for 3600 s.

3. RESULTS AND DISCUSSION

3.1 Catalyst structure, morphology and composition

XRD measurements were conducted for structure and phase analysis of different catalysts, as shown in Fig. 1. The diffraction peak at 24.6 ° is associated with (002) plane of the carbon support. The diffraction peaks of the PtRu/C catalysts at 38.9 °, 67.8 ° and 82.1 ° are attributed to Pt(111), Pt(220) and Pt(311) plane, respectively, according to XRD peak analysis software of X'Pert Highscore (Reference code: 00-001-1190). It indicates that Ru atoms were dissolved in the Pt lattice to form a substitution solid solution during the chemical reduction of Ru³⁺ and Pt⁴⁺ in ethylene glycol. For the pristine PtRu/C catalyst, Pt(220) and Pt(311) diffraction peaks are very weak because of small particle size of 1.7 nm (Fig. 2). Bock et. al. have compared XRD patterns of PtRu/C catalysts with different particle size, which became broader with the smaller particle size [20]. It can be expected by Scherrer's equation which can be used to calculate the mean particle size of nanoparticles roughly according to half width of diffraction peak [24]. The XRD peaks of annealed catalysts shifts towards higher 2θ values, indicative of the decreased lattice parameter and improved alloy degree after reduction treatment [25]. The similar relationship between alloying degree and diffraction angle was also observed by Pires et. al., who calculated the alloying degree of PtRu/C on the basis of XRD data according to Vegard's Law when studying the effect of alloying degree on ethanol electro-oxidation activity [26]. Moreover, the diffraction peaks become sharp and intensities are enhanced with increasing of reducing temperature. It could be caused by the formation of grain boundary and particle agglomeration [27, 28].

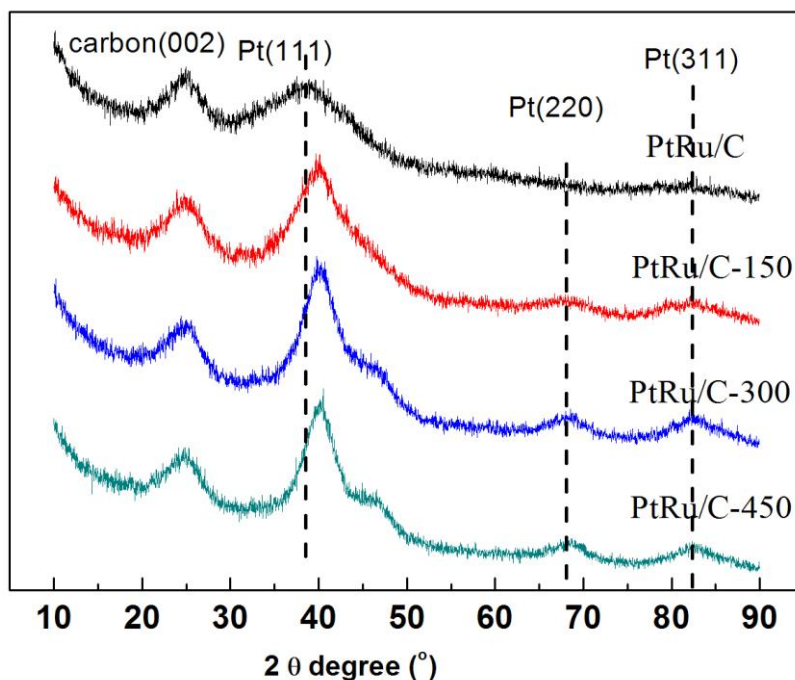


Figure 1. XRD patterns of PtRu/C catalysts treated in H₂ atmosphere at different temperatures

Fig. 2 shows TEM images of different catalysts. It can be seen from Fig. 2a, d, h and k that PtRu nanoparticles are distributed uniformly on carbon support and particle size distributions were calculated according to the statistics of more than 200 particles. As shown in Fig. 2c, the average particle size of pristine PtRu/C is only 1.7 nm. The particle size increases obviously after reduction treatment, and it is 2.8 nm, 2.5 nm and 3.2 nm for PtRu/C-150, PtRu/C-300 and PtRu/C-450 catalysts, as shown in Fig. 2f, j, m, respectively. The relative proportion of small particles (< 1.5 nm) decreases with increasing of reduction temperature from 42 % of pristine PtRu/C to 0.36 % of PtRu/C-300, and zero for PtRu/C-450. There is little difference of average particle size between PtRu/C-150 and PtRu/C-300, indicating that the reduction treatment at 300 °C does not lead to further increase in particle size. Combined the analysis of performance data of CO and methanol electro-oxidation in the following paragraphs, there may be another change for the PtRu nanoparticles on the PtRu/C-300 catalyst since it shows much higher electro-catalytic activity. Considering the relative distribution of large particles, which is larger than 3.5 nm, it is about 17 %, 3 % and 26 % for PtRu/C-150, PtRu/C-300 and PtRu/C-450, respectively. It could be concluded that the nanoparticles interconnected and grain boundary formed [29]. From the high resolution TEM images it can be seen that the crystal lattice fringes clearly, which is assigned to the crystalline face of the Pt(111) are 0.225 nm, 0.226 nm and 0.228 nm for the PtRu/C-150, PtRu/C-300 and PtRu/C-450 catalysts, respectively, smaller than 0.231 nm of pristine PtRu/C catalyst due to the lattice contraction upon alloying.

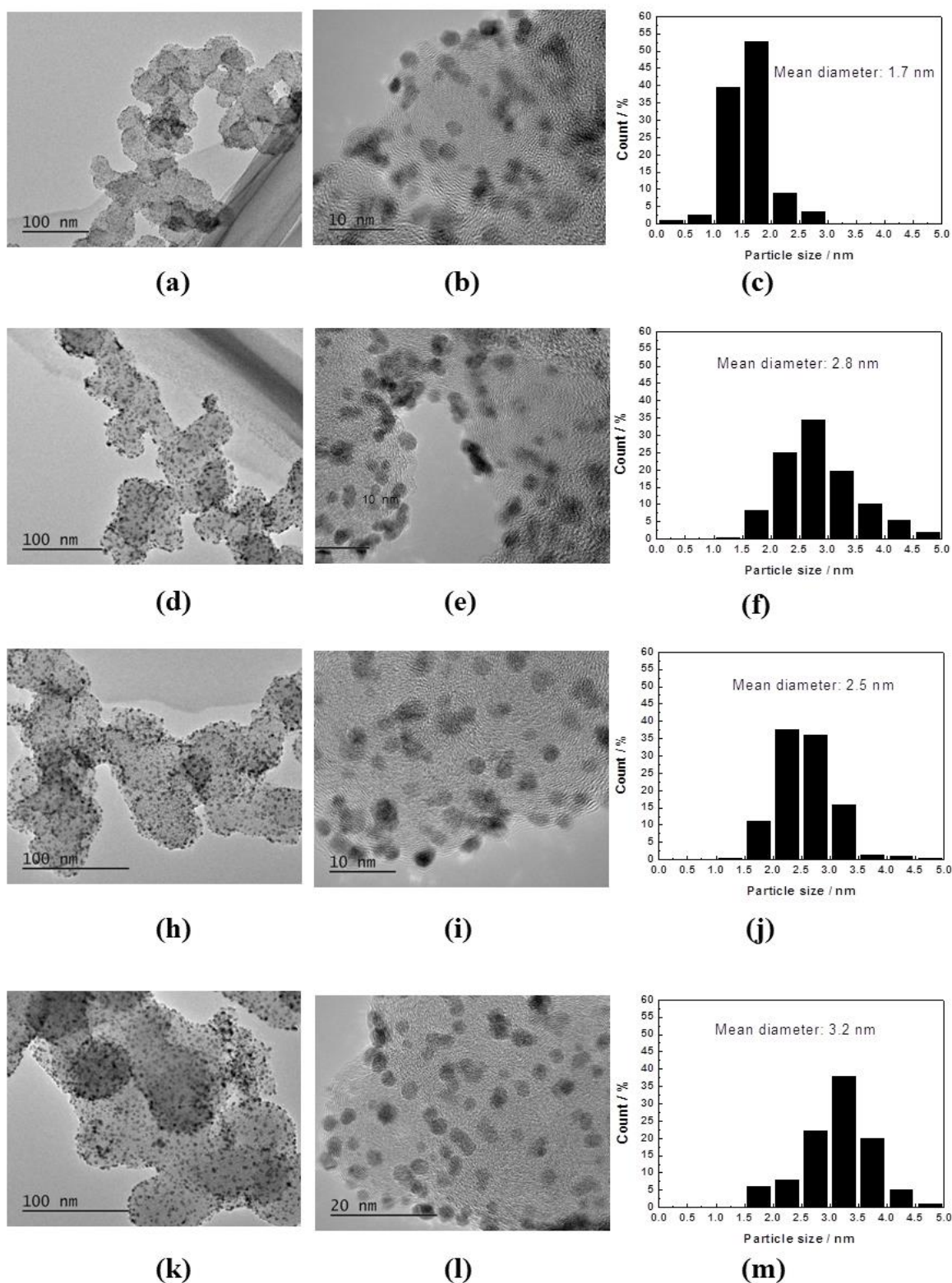


Figure 2. TEM images and the corresponding particle size histogram. (a), (b) and (c) for PtRu/C catalyst, (d), (e) and (f) for PtRu/C-150, (h), (i) and (j) for PtRu/C-300, and (k), (l) and (m) for PtRu/C-450.

Fig. 3 shows the EDS mappings of Pt and Ru element in the PtRu/C catalysts under STEM mode. Mapping EDS scan shows that the signal of Pt, Ru, C and Cu. The signal of Cu comes from copper grid, which supports the catalyst sample during imaging. It can be seen that the distribution of Pt and Ru elements is very strong and accordance with the photograph in box, exhibiting a uniform distribution of Pt and Ru atoms in the catalyst particles. Table1 lists the content of Pt and Ru element in the catalyst of PtRu/C. The relative content of Pt and Ru is 67 % and 33 %, which is very close to the nominal ratio of 2:1 (Pt:Ru), and corresponding to the 68 % and 32 % results measured with ICP-OES.

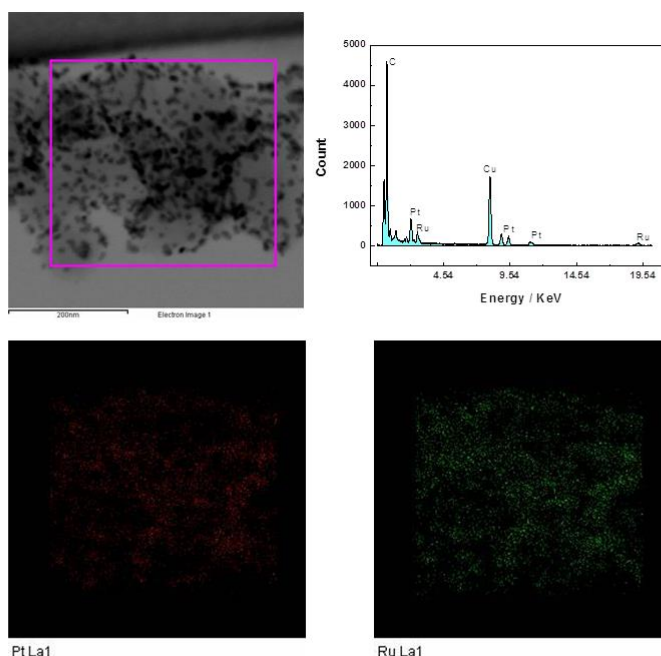


Figure 3. EDS mapping scan of PtRu/C catalyst

Table 1. The composition of PtRu/C catalyst by EDS and ICP-OES

Element		Pt	Ru
Content (at. %)	EDS	67 %	33 %
	ICP	68 %	32 %
Content (wt. %)	EDS	78 %	22 %
	ICP	80 %	20 %

3.2 Thermal analysis of catalysts

Simultaneous thermal analysis was used to observe the changes of weight and heat effect of the catalysts during temperature programmed. It can be seen from Fig. 4 that there is an obvious mass loss of 9 % for untreated PtRu/C catalyst, which is according to an exothermic peak of differential scanning calorimetry (DSC) curve at 110 °C due to the thermal decomposition of adsorbed species on the catalyst. For PtRu/C-150 catalyst, there is still 8 % mass loss and DSC curve shows a wide exothermic peak. After reduction treatment at 300 °C, the mass loss and exothermic peak decrease obviously, similar to the catalyst of PtRu-450, indicating that most of the adsorbed species have been removed.

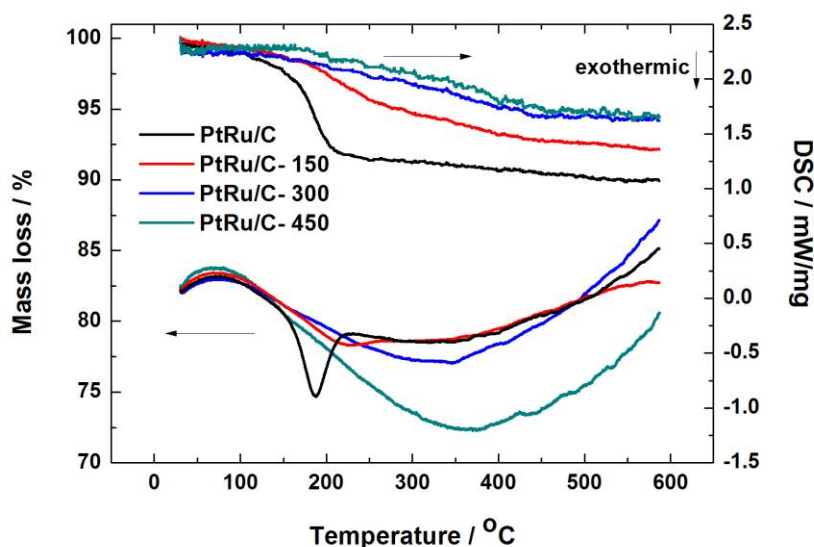


Figure 4. STA curves for different catalysts before and after reducing treatment

3.2 Electro-catalytic activities

CO stripping voltammetry has been used to evaluate CO electro-oxidation activity since CO as the main adsorbate on catalyst surface [10]. Fig. 5 shows CO stripping curves which recorded in 0.1 mol L⁻¹ HClO₄ with 20 mV s⁻¹ scan rate. It can be seen that the electro-oxidation activities of adsorbed CO (CO_{ads}) are improved obviously for the catalysts after reduction treatment. The onset potential shifts negatively about 0.04 V and 0.09 V for PtRu/C-150 and PtRu/C-300 catalysts, respectively, compared to the pristine PtRu/C catalyst. PtRu/C-300 catalyst exhibits the highest activity for CO electro-oxidation, which occurs at 0.44 V and centres at 0.58 V, although peak current slightly lower than that of PtRu/C-150 catalyst. This trend agrees with the reported data that the CO stripping peak showed negative shift as PtRu alloy degree increasing [30]. In consideration of particle size distribution of PtRu/C-150 and PtRu/C-300 catalysts, the improved activity for CO tolerance also maybe due to the formation of grain boundary of the particles. Wang et. al. observed that grain boundary would be generated during heat treatment, which served as the active sites for methanol electro-oxidation [27]. When the treatment temperature increases further to 450 °C, onset potential and

peak potential both shift positively during CO stripping due to the particle agglomeration during annealing, compared with PtRu/C-300.

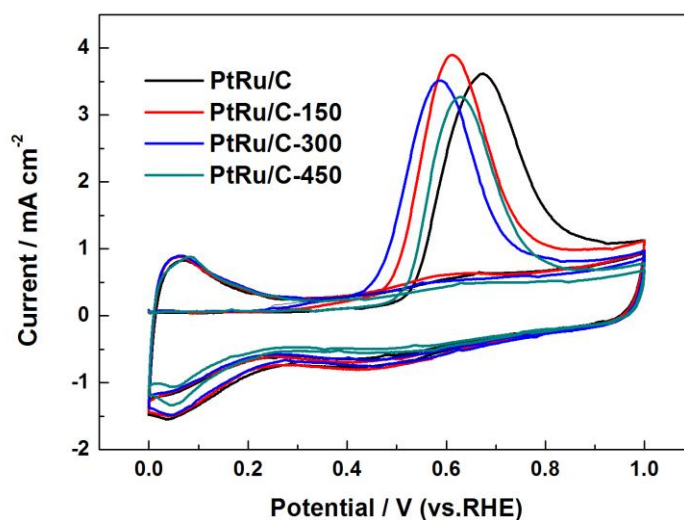


Figure 5. CO stripping curves of the catalysts in $0.1 \text{ mol L}^{-1} \text{ HClO}_4$ with a scan rate of 20 mV s^{-1} .

The electro-catalytic activities for methanol electro-oxidation over the catalysts are shown in Fig. 6. LSV curves were recorded at a slow scan rate of 1 mV s^{-1} . Below 0.35 V , current density shows zero because of the adsorption of the species dissociated from methanol on the catalyst surface. Methanol electro-oxidation on PtRu/C catalyst occurs at about 0.43 V , where the dissociation of water produces oxidizing species such as $-\text{OH}_{\text{ads}}$. It facilitates oxidation of CO_{ads} and inhibits methanol adsorption, resulting in the oxidation current density increases rapidly with potential increasing. The onset of methanol electro-oxidation shifts negatively significantly on the catalysts after reduction treatment, which at ca. 0.40 V , 0.39 V and 0.42 V for PtRu/C-150, PtRu/C-300 and PtRu/C-450 catalysts, respectively. In addition, methanol electro-oxidation current of the annealed catalysts is much higher than that of pristine PtRu/C catalyst, especially on the PtRu/C-300 catalyst. It demonstrates that the catalytic activity is much superior towards methanol electro-oxidation for PtRu/C-300 than the other catalysts which depending on its increased PtRu alloy degree and grain boundaries as well as the electrochemical active area. During the process of methanol electro-oxidation, the possible rate determining rate step was the reaction of CO_{ads} with Ru oxide on PtRu/C catalyst surface [31]. Thus the role of PtRu alloy degree is important when the CO_{ads} shifts to the Pt active sites which adjacent to $\text{Ru-OH}_{\text{ads}}$ considering bifunctional mechanism. Based on previous studies, it was found that anodic treatment in acid environment could improve the catalytic activity for methanol electro-oxidation based on the consideration of irreversible Ru oxides decreasing and reversible Ru oxides increasing [32]. For the PtRu/C catalyst prepared by ethylene glycol method, there should be some Ru oxides, such as RuO and RuO₂. Reductive treatment at high temperature can reduce Ru oxides from high valence to zero or low valence, and serves as the reversible and beneficial species. The chronoamperometry curve at 0.7 V was used to evaluate the catalyst stability for methanol electro-oxidation. The oxidation current becomes stable with time increasing. The stable current is 0.11 mA for PtRu/C catalyst, which is much lower than the catalysts with reduction treatment. PtRu/C-300

catalyst exhibits the highest current at the beginning of time. While after 2650 s, the current down to 0.46 mA, lower than that of PtRu/C-150 catalyst. PtRu/C-150 catalyst decays slowest and shows the highest stability for methanol electro-oxidation among the catalysts.

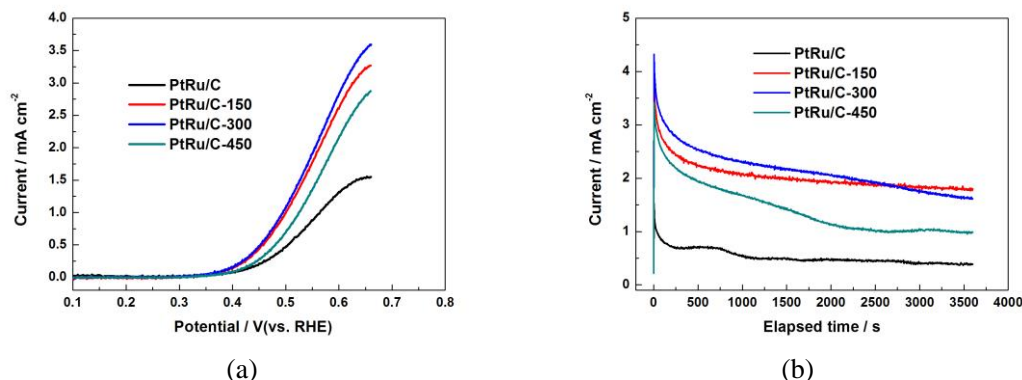


Figure 6. (a) LSV curves with a scan rate of 1 mV s^{-1} and (b) Chronoamperometry curves at 0.7 V of the catalysts in $0.1 \text{ mol L}^{-1} \text{ HClO}_4 + 0.5 \text{ mol L}^{-1} \text{ CH}_3\text{OH}$

4. CONCLUSIONS

PtRu/C catalysts were prepared by the modified ethylene glycol method followed with reduction treatment at different temperatures. The alloy degree of PtRu/C catalysts was improved with an increase in crystalline size after reduction treatment. PtRu/C-300 catalyst showed the highest activity for CO and methanol electro-oxidation due to the removal of surface adsorbates, the increase of alloy degree and electrochemical surface area, as well as the formation of grain boundary among the interconnect particles.

ACKNOWLEDGEMENTS

This work was financially supported by the project of National Scientific Fund of China (Grant No. 21403023).

References

1. S. C. Thomas, X. M. Ren, S. Gottsfeld, P. Zelenay, *Electrochim. Acta*, 47(2002)3741.
2. N. Jung, D. Y. Chung, J. Ryu, S. J. Yoo, Y. E. Sung, *Nano Today*, 9(2014)433
3. B. C. H. Steele, A. Heinzl, *Nature*, 414(2001)345
4. Z. D. Wei, S. H. Chan, *J. Electroanal. Chem.*, 569(2004)23.
5. E. A. Batista, H. Hoster, T. Iwasita, *J. Electroanal. Chem.*, 554(2003)265.
6. L. Zhang, J. Kim, H. M. Chen, F. Nan, K. Dudeck, R. S. Liu, *J. Power Sources*, 196(2011)9117
7. T. Takeguchi, T. Yamanaka, K. Asakura, E. N. Muhamad, K. Uosaki, W. Ueda, *J. Am. Chem. Soc.*, 134(2012)14508.
8. X. H. Jian, D. S. Tsai, W. H. Chung, Y. S. Huang, F. J. Liu, *J. Mater. Chem.*, 19(2009)1601.
9. E. A. Batista, H. Hoster, T. Iwasita, *J. Electroanal. Chem.*, 554(2003)265.
10. Q. Wang, G. Q. Sun, L. H. Jiang, Q. Xin, S. G. Sun, Y. X. Jiang, S. P. Chen, Z. Jusys, R. J. Behm,

- Phys. Chem. Chem. Phys.*, 9(2007)2686.
11. A. U. Nilekar, K. Sasaki, C. A. Farberow, R. R. Adzic, M. Mavrikakis, *J. Am. Chem. Soc.*, 133(2011)18574.
 12. J. Melke, A. Schoekel, D. Dixon, C. Cremers, D. E. Ramaker, C. Roth, *J. Phys. Chem. C*, 114(2010)5914.
 13. C. Roth, N. Benker, T. Buhrmester, M. Mazurek, M. Loster, H. Fuess, D. C. Koningsberger, D. E. Ramaker, *J. Am. Chem. Soc.*, 127(2005)14607.
 14. J. S. Guo, G. Q. Sun, Q. Wang, G. X. Wang, Z.H. Zhou, S. H. Tang, L. H. Jiang, B. Zhou, Q. Xin, *Carbon*, 44(2006)152.
 15. J. Xie, X. Yang, X. Xu, C. Yang, *Int. J. Electrochem. Sci.*, 12(2016)466.
 16. G. Wang, T. Takeguchi, T. Yamanaka, E. N. Muhamad, M. Mastuda, W. Ueda, *Appl. Catal. B: Environ.*, 98(2010)86.
 17. Z.D. Wei, Y.C. Feng, L. Li, M.J. Liao, Y. Fu, C.X. Sun, Z.G. Shao, P.K. Shen, *J. Power Sources*, 180 (2008) 84.
 18. K. S. Kadakia, M. K. Datta, O. I. Velikokhatnyi, P. J. Hanumantha, S. K. Park, S. J. Chung, D. H. Hong, J. A. Poston, A. Manivanan, P. N. Kumta, *J. Electrochem. Soc.*, 161 (10) F1053-F1060 (2014).
 19. P.A. Christensen, A. Hamnett, *J. Electroanal. Chem. Interfac.*, 260(1989)347.
 20. C. Bock, C. Paquet, M. Couillard, G. A. Botton, B. R. MacDougall, *J. Am. Chem. Soc.*, 126 (2004) 8028.
 21. Q. Wang, X. Lu, Q. Xin, G. Q. Sun, *Chinese J. Catal.*, 35(2014)1394.
 22. J. Melke, A. Schoekel, D. Dixon, C. Cremers, D. E. Ramaker, C. Roth, *J. Phys. Chem. C*, 114(2010) 5914.
 23. Q. Wang, H. L. Tao, Z. Q. Li, C. H. Chen, S. S. Liu, L. Han, X. Lu, *J. Energ. Chem.*, 25 (2016) 811.
 24. A. Monshi, M. R. Foroughi, M. R. Monshi, *World J. Nano Sci. Eng.*, 2 (2012) 154.
 25. S. Y. Yan, G. Q. Sun, J. Qi, Y. Gao, Q. Xin, *Chinese J. Catalysis*, 30(2009)1109.
 26. F. I. Pires, P. G. Corradini, V. A. Paganin, E. Antolini, J. Perez, *Ionics*, 19 (2013) 1037.
 27. G. Wang, T. Takeguchi, E. N. Muhamad, T. Yamanaka, W. Ueda, *Int. J. Hydrogen Energ.*, 36(2011)3322.
 28. M. Tsyppkin, J. L. G. Fuente, S. G. Rodriguez, Y. Yu, P. Ochal, F. Seland, O. Safonova, N. Muthuswamy, M. Ronning, D. Chen, S. Sunde, *J. Electroanal. Chem.*, 704 (2013) 57.
 29. H. V. Swygenhoven, D. Farkas, A. Caro, *Phys. Rev. B*, 62 (2000) 831.
 30. G. Wang, T. Takeguchi, E. N. Muhamad, T. Yamanaka, M. Sadakane, W. Ueda, *J. Electrochem. Soc.*, 156 (2009) B1348.
 31. T. Iwasita, H. Hoster, A. John-Anacker, W. F. Lin, W. Vielstich, *Langmuir*, 16 (2000) 522.
 32. Q. Lu, B. Yang, L. Zhuang, J. Lu, *J. Phys. Chem. B*, 109 (2005) 1715.